RSC Advances

PAPER

View Article Online
View Journal | View Issue

Cite this: *RSC Adv.*, 2018, **8**, 24970

Functional polyaspartic acid derivatives as eco-friendly corrosion inhibitors for mild steel in 0.5 M H_2SO_4 solution

Chunxiao Chai,[a] Yanhua Xu,[a] Shuchen Shi,[a] Xiaowei Zhao,[ab] Yufeng Wu,[ab] Ying Xu [ab] and Lei Zhang *[ac]

Received 24th April 2018
Accepted 3rd July 2018

DOI: 10.1039/c8ra03534b

rsc.li/rsc-advances

To improve the corrosion inhibition efficiency of eco-friendly polyaspartic acid (PASP) for mild steel in acidic solutions, PASP/*N*-(3-aminopropyl)imidazole (PD-1) and PASP/*N*-(3-aminopropyl)-imidazole-*co*-*n*-dodecylamine (PD-2) were chemically synthesized by the facile ring-opening reaction of polysuccinimide. Inhibition efficiencies of PD-1 and PD-2 for mild steel in a 0.5 M H_2SO_4 solution were investigated by electrochemical measurements (electrochemical impedance and polarization) and the weight loss method. In comparison with PASP, PD-1 and PD-2 show improved inhibition efficiencies due to the functional groups. In particular, PD-2 shows superior corrosion inhibition capacity, and the efficiency is up to 94% at a relatively low concentration of 100 mg L^{-1} at 298 K, as determined by potentiodynamic polarization measurements. Surface analysis of mild steel with PD-2 as an inhibitor clearly indicates that the inhibitor molecules adsorb on the steel surface and efficiently inhibit the corrosion of mild steel. The present work provides very meaningful results in designing and preparing new polymer inhibitors with high inhibition efficiency.

1. Introduction

It is well-known that acidic solutions are widely used in chemical industries such as acid cleaning, de-scaling, pickling, *etc.*, and corrosion inhibitors are indispensable for inhibiting metal corrosion during these industrial processes.[1–5] Most well-known acid inhibitors are organic compounds containing heteroatoms (N, S and/or O) and these compounds are active against metal corrosion by adsorbing on the metal surface. Up to now, a variety of corrosion inhibitors containing Schiff base,[6,7] pyrimidine,[8,9] azoles[10–14] and other heterocycles[15,16] have been reported. Previous studies have also indicated that organic compounds containing unsaturated bonds[17] or long alkyl chains[10] showed good corrosion inhibition properties for steel.

With the enhancement of environmental consciousness, designing eco-friendly corrosion inhibitors has gained tremendous momentum.[18–22] Due to the features of non-toxicity and high safety, green polymer inhibitors have attracted much attention. An overview on the use of carbohydrate polymers as corrosion inhibitors for metal materials in different media has been summarized by Umoren and Eduok.[23] In that article, exudate gums, cellulose, starch, chitosan, *etc.*, and their derivatives were enumerated. Polymeric structures used as corrosion inhibitors for the oil and gas industry have also attracted much attention.[24] Recently, Mobin *et al.* reported on the inhibition performance of polysaccharide from Plantago for carbon steel corrosion in 1 M HCl and an efficiency of 92.53% at 1000 mg L^{-1} was obtained.[25] Amino acid-modified konjac glucomannan was also evaluated as a corrosion inhibitor in 0.5 M HCl solution by Yang *et al.* and an efficiency of 92.4% was achieved at 2000 mg L^{-1}.[26] Notably, large dosages are often necessary to achieve high inhibition efficiencies for most polymers inhibitors.[27–29] Therefore, developing new eco-friendly polymer inhibitors with high-efficiency at low concentrations is particularly meaningful.

Polyaspartic acid (PASP) is a well-known, eco-friendly, and biodegradable polymer that exists naturally in the shell of mollusks. Currently, tons of PASP can be obtained by chemical synthesis. PASP is generally considered as a new type of green water treatment agent, particularly as a scale inhibitor.[30] In addition, the corrosion inhibition performances of PAPS or derivatives for mild steel,[31] WE43 magnesium alloy,[32] and A3 carbon steel[33] in 3.5% NaCl solution have been studied. Meanwhile, the efficiency of PASP as a pickling corrosion inhibitor for carbon steel in 0.565 M H_2SO_4 solutions was investigated by Cui *et al.* and a moderate efficiency of 80.33% was obtained at an extremely high concentration of 6 g L^{-1} at 283 K.[34] Investigations by Qian *et al.* also showed that the

[a]*College of Chemistry and Chemical Engineering, Henan University, Kaifeng 475004, PR China. E-mail: hndxzhanglei606@126.com*

[b]*Henan Engineering Research Center of Industrial Circulating Water Treatment, Kaifeng 475004, PR China*

[c]*Department of Chemistry, Key Laboratory for Preparation and Application of Ordered Structural Materials of Guangdong Province, Shantou University, Shantou, Guangdong 515063, P. R. China*

inhibition efficiency of PASP for mild steel in 0.5 M H_2SO_4 solution was limited when PASP was used independently.[35] With addition of I^- ion into the test solution, the inhibition efficiency was enhanced because of the synergistic effect. Nevertheless, chemical modification by the introduction of functional groups into the molecular structure may be a more effective pathway to improve the inhibition property of PASP for metals in acid solution.

Based on above analysis, *N*-(3-aminopropyl)imidazole was first adopted as a modifier to prepare the novel PASP derivative (PD-1) by considering that the group of the imidazole ring has a strong adsorption ability on metal surface.[11] Furthermore, *n*-dodecylamine was adopted as a co-modifier to generate another PASP derivative (PD-2), since it is known that the inhibition efficiency could be enhanced by introducing alkyl chains into the molecular structure of the inhibitor.[36] Then, the corrosion inhibition efficiencies of PD-1 and PD-2 for mild steel in 0.5 M H_2SO_4 were evaluated by electrochemical measurements and weight loss method with concentrations ranging from 5 to 100 mg L^{-1}. To investigate the adsorption type of PD-1 and PD-2 on the steel surface, the thermodynamic parameters of the adsorption isotherms were analyzed. The relationship between the molecular structure and the inhibition mechanism was also discussed.

2. Experimental

2.1. Materials

All reagents were of analytical grade and used without further purification. *N*-(3-aminopropyl)-imidazole and *n*-dodecylamine were acquired from Energy Chemical (Shang Hai). Sulfuric acid was purchased from Kaifeng Dongda Chemical Industry Co., Ltd. The composition (wt%) of the selected $20^{\#}$ mild steel sample used in the present work was C (0.17%), Si (0.17%), Mn (0.35%), Cr (0.25%), (Ni 0.30%), Cu (0.25%) and Fe balance, which was purchased from Jiangsu Xinyou Instrument Factory.

2.2. Preparations of PD-1 and PD-2

First, polysuccinimide was synthesized referring a previous literature.[30] PD-1 was prepared according to the following procedures. Briefly, polysuccinimide (1.9 g), *N*-(3-aminopropyl) imidazole (2.5 mL) and distilled water (5 mL) were introduced into a 100 mL three-necked flask. The reaction mixture was heated to 333 K and stirred for 24 h. Then, the mixture was cooled to room temperature and poured into 200 mL of acetone to generate a precipitate. The precipitate was dried under vacuum at 353 K for 24 h to obtain the target PASP derivative (PD-1).

Polysuccinimide (1.9 g), which was pre-dissolved in *N*, *N*-dimethylformamide (5 mL), was introduced into a 100 mL round-bottom flask, followed by the addition of *N*-(3-aminopropyl)-imidazole (1.25 mL) and *n*-dodecylamine (1.8 g). The resultant mixture was heated to 333 K and stirred for 24 h. Then, the mixture was cooled to room temperature and poured into 200 mL of acetone. The obtained precipitate was dried under vacuum at 353 K for 24 h to obtain another PASP derivative (PD-2). The synthetic routes of PD-1 and PD-2 are shown in Scheme 1.

2.3. Structural characterizations of PD-1 and PD-2

Structural characterizations of PD-1 and PD-2 were performed by ^{1}H NMR spectrum (AVANCE 400 MHz NMR spectrometer, Bruker Instruments, Germany) and Fourier transform infrared spectroscopy (VERTEX 70 FTIR spectrometer, Bruker Instruments, Germany).

2.4. Electrochemical measurements

Electrochemical measurements were carried out in a 0.5 M H_2SO_4 solution without and with (5, 10, 20, 50, 100 mg L^{-1} of PD-1 and PD-2, respectively) at 298 K using a CHI 660E electrochemical system (Shanghai Chenhua Instrument Co., Ltd). All measurements were carried out in a conventional three-electrode cell assembly. A platinum sheet (2 cm^2 area) and saturated calomel electrode (SCE) were utilized as the counter electrode and reference electrode, respectively. The disc-type working electrode (WE) with an exposed area of 1 cm^2 was made of $20^{\#}$ mild steel mounted in epoxy resin. Prior to all tests, the surface of the working electrode was ground with polishing paper with abrasive paper (400 grit, 600 grit, 1200 grit, and 2000 grit, Dongguan Golden Sun abrasives CO., Ltd), rinsed with distilled water, degreased with acetone and dried. Then, the working electrode was immersed in the test solution for 1 h to obtain a stable open-circuit potential (OCP). A frequency range of 100 KHz to 0.1 Hz with the amplitude of 10 mV at a stable OCP was applied to the EIS measurements. The impedance data

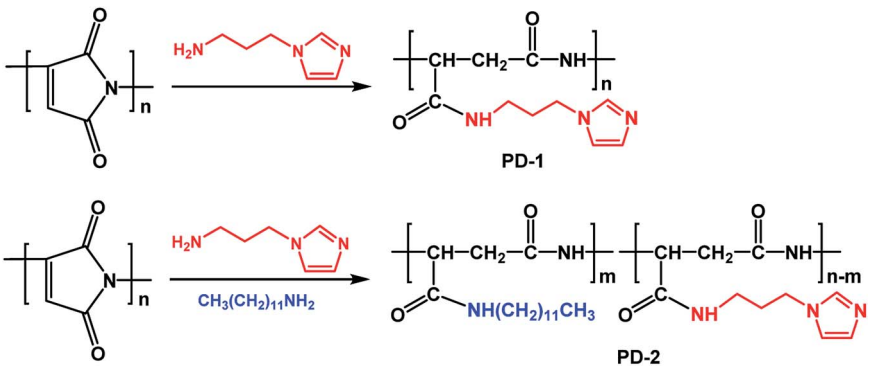

Scheme 1 Synthetic routes of PD-1 and PD-2.

were analyzed using ZView 2 software. Potentiodynamic polarization curves were measured in the potential range of ±250 mV *versus* OCP at a potential sweep rate of 1 mV s^{-1}. Inhibition efficiencies (IE_P and IE_E) from the polarization curves and EIS were calculated according to the corrosion current density (i_{corr}) and charge transfer resistance (R_{ct}) values, respectively.

2.5. Weight-loss test

Weight-loss tests were carried out in a 0.5 M H_2SO_4 solution at 298 K in the absence and presence of various concentrations (5, 10, 20, 50, 100 mg L^{-1}) of PD-1 and PD-2. Prior to all tests, mild steel sheets of 5 × 2.5 × 0.2 cm were washed with water and acetone. After drying and accurate weighing, the mild steel sheets were immersed in 500 mL of a 0.5 M H_2SO_4 solution for 12 h at 298 K with and without inhibitors. Then, the specimens were taken out and washed with distilled water and acetone; and subsequently dried and weighed again. The experiments were carried out in triplicates to achieve good reproducibility, and the average weight loss was utilized to calculate the corrosion rate (ν_{corr}) and inhibition efficiency (IE_W).

2.6. Surface analysis

Scanning electron microscopy (SEM) and energy dispersive X-ray spectroscopy (EDX) measurements of the mild steel surface were performed using a Hitachi model SU 8020 field emission scanning electron microscope (Hitachi, Japan). X-ray photoelectron spectroscopy (XPS) measurements were carried out on an ESCALAB 250Xi XPS system (Thermo Fisher Scientific Corporation, America) employing Al K_α as the incident radiation source (1486.6 eV). The binding energy of C 1s (284.8 eV) was used as a reference.

3. Results and discussion

3.1. Characterizations of PD-1 and PD-2

3.1.1 FTIR spectral analysis. FTIR spectra of synthesized PD-1 and PD-2 are shown in Fig. 1. Compared to the IR spectrum of polysuccinimide shown in other literature,[37] the stretching vibration of the carbonyl of imide at 1715 cm^{-1} disappears. Meanwhile, the strong characteristic peaks at 1655 cm^{-1} in the spectra of PD-1 and PD-2 are attributed to the carbonyl stretching vibration of amide. These results indicate that the ring-opening reaction of polysuccinimide was performed successfully. The peaks at 1109 and 1084 cm^{-1} in the spectrum of PD-1 are ascribed to the stretching vibration of the imidazole ring. Therefore, the imidazole group was bonded onto the polymer chain by a ring-opening reaction of *N*-(3-aminopropyl)imidazole with polysuccinimide. In the IR spectrum of PD-2, apart from the vibrations (1110 and 1086 cm^{-1}) of the imidazole ring, the peaks at 2926 and 2854 cm^{-1} are ascribed to the asymmetric and symmetric stretching vibrations of the alkyl chain, respectively. As a result, both *N*-(3-aminopropyl)imidazole and *n*-hexylamine were involved in the preparation of PD-2.

3.1.2. ^{1}H NMR spectral analysis. Fig. 2 shows the ^{1}H NMR spectra of PD-1 and PD-2 in D_2O. From the spectrum of PD-1, in addition to the signals of –CH– (δ_H = 4.2–4.7) and –CH_2– (δ_H = 2.4–3.0) attributed to the PASP chains,[38] signals at δ_H = 7.7, δ_H = 7.1 and δ_H = 6.9 are ascribed to various protons in the imidazole ring. Meanwhile, the peaks at δ_H = 3.9, δ_H = 3.0 and δ_H = 1.9 are ascribed to different methylene protons in the *N*-(3-aminopropyl)imidazole group. In addition to the similar peaks with PD-1, other peaks located at high field in ^{1}H NMR spectrum of PD-2 are attributed to various protons in the *n*-dodecyl group. Therefore, the imidazole ring and *n*-dodecyl group are bonded onto the polymer chains in PD-2. Combined with previous analysis of FTIR spectra, it can be concluded that the PASP derivatives, PD-1 and PD-2, were successfully synthesized.

3.2. Electrochemical measurements

3.2.1. Open-circuit potential (OCP) – time curves. A stable potential without an external current applied on the mild steel working electrode surface is important for potentiodynamic polarization and EIS measurements. Fig. 3 reveals the plots of open circuit potential (*versus* SCE reference electrode) in 0.5 M H_2SO_4 solution as a function of immersion time without and with various concentrations of inhibitors at 298 K. For PD-1 and PD-2 at various concentrations, different exposure times were required to achieve a steady OCP value. However, it is clearly seen from Fig. 3 that 1 h was enough to get a steady potential and, therefore, was utilized as the immersion time before potentiodynamic polarization and EIS measurements.

3.2.2. Potentiodynamic polarization measurements. The potentiodynamic polarization curves of the mild steel working electrode in 0.5 M H_2SO_4 solution without and with inhibitors were recorded and are shown in Fig. 4. With PD-1 as an inhibitor, the cathodic curves move toward a lower current density region, while the variations of anodic curves are not obvious. This phenomenon suggests that an efficient adsorption layer on the mild steel surface is formed and the hydrogen ion reduction is retarded.[39] It should be stressed that both a noticeable anodic and cathodic shift significantly to lower current densities with

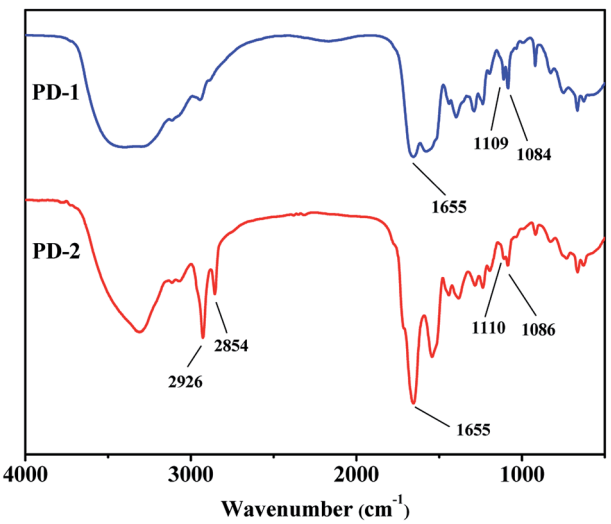

Fig. 1 FTIR spectra of PD-1 and PD-2.

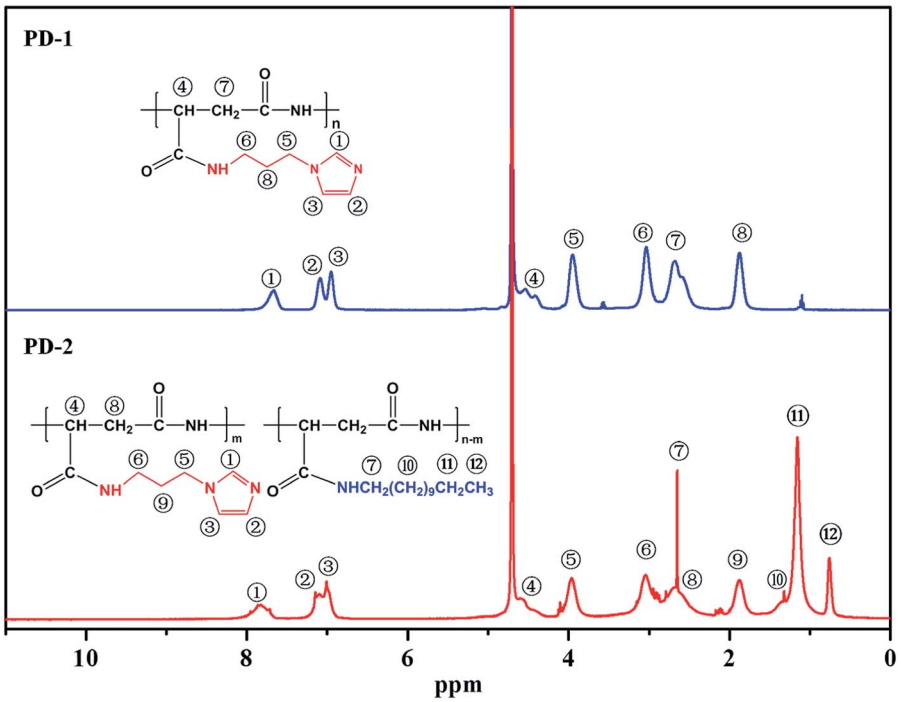

Fig. 2 ^{1}H NMR spectra of PD-1 and PD-2.

PD-2 as an inhibitor, which indicates that PD-2 shows superior efficiency for retarding the corrosion of mild steel in acidic solutions.

The related electrochemical parameters, such as the corrosion potential (E_{corr}), anodic Tafel slope (β_a), cathodic Tafel slope (β_c), linear polarization resistance (R_p)and corrosion current density (i_{corr}) calculated from the polarization curves, are listed in Table 1. The inhibition efficiency (IE_P) and the surface coverage (θ) were calculated according to the following eqn (1) and (2):

$$IE_P(\%) = \frac{i^0_{corr} - i_{corr}}{i^0_{corr}} \times 100 \quad (1)$$

$$\theta = \frac{IE_P(\%)}{100} \quad (2)$$

where i^0_{corr} and i_{corr} are the current densities of uninhibited and inhibited mild steel working electrodes, respectively. It is seen from Table 1 that the shift of the E_{corr} (ΔE_{corr}) values is lower than 85 mV in each case, suggesting that PD-1 and PD-2 are mixed-type inhibitors.[40] The value of the current density decreases from 2.232 mA cm^{-2} for the blank to 0.621 mA cm^{-2} in the presence of 5 mg L^{-1} PD-1, and it further decreased to 0.237 mA cm^{-2} for 100 mg L^{-1} PD-1. The inhibition efficiencies of PD-1 calculated by eqn (1) are 72.2% and 89.4% at the concentrations of 5 mg L^{-1} and 100 mg L^{-1}, respectively. By comparing the results in other literatures,[34,35] the inhibition efficiency of PD-1 is obviously higher than that of PASP. The enhanced inhibition ability may be ascribed to the bonded functional imidazole ring due to the additional donor–acceptor interaction between the π-electrons and the vacant d-orbitals of Fe atoms.

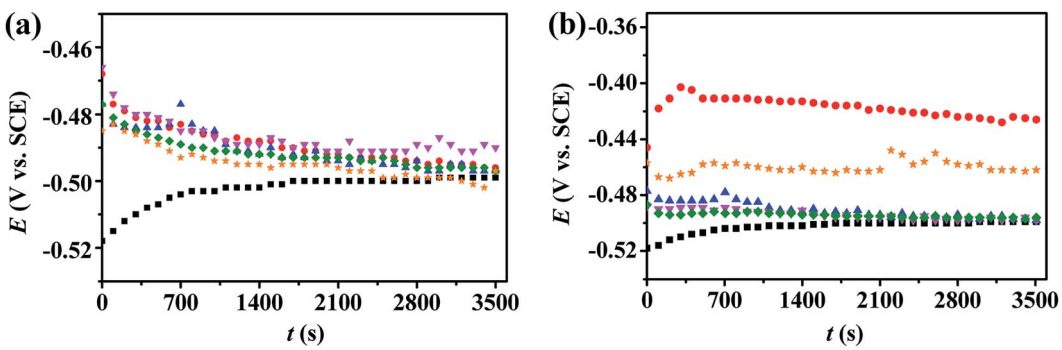

Fig. 3 Open circuit potential *versus* time curves in 0.5 M H_2SO_4 solution at 298 K without (■) and with different concentrations of PD-1 (a) and PD-2 (b): 5 mg L^{-1} (●), 10 mg L^{-1} (▲), 20 mg L^{-1} (▼), 50 mg L^{-1} (◆) and 100 mg L^{-1} (★).

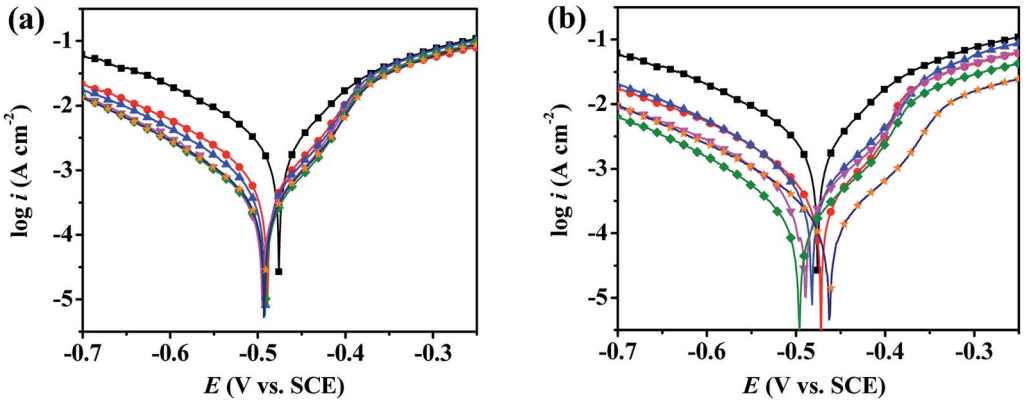

Fig. 4 Potentiodynamic polarization curves for mild steel in 0.5 M H_2SO_4 solution without (■) and with different concentrations of PD-1 (a) and PD-2 (b) at 298 K. Inhibitor concentration: 5 mg L^{-1} (●), 10 mg L^{-1} (▲), 20 mg L^{-1} (▼), 50 mg L^{-1} (◆) and 100 mg L^{-1} (★).

To minimize the environmental impacts, it is important to develop high-efficiency inhibitors with low dosage. Singh *et al.* found that an acceptable efficiency (80.7%) of polyacrylamide grafted with okra mucilage for mild steel in 0.5 M H_2SO_4 solution can be achieved at an extremely low concentration of 5 mg L^{-1}.[41] Since it has been reported on that long-chain alkyl substituents greatly benefit the inhibition efficiency of inhibitors,[10,42] *n*-dodecylamine was selected as a co-modifier and another PASP derivative (PD-2) were prepared. Notably, the inhibition efficiency of PD-2 for mild steel in 0.5 M H_2SO_4 solution was up to 84.1% at a low concentration of 5 mg L^{-1}, and a high efficiency of 94.0% can be achieved at a concentration of 100 mg L^{-1}. In contrast to other polymer inhibitors,[25–29,43,44] the PASP derivative PD-2 demonstrates better inhibition efficiency at low concentrations. The limited inhibition efficiency of PASP in 0.5 M H_2SO_4 solution may be ascribed to the weak interaction of the PASP chains with the metal surface. By introducing functional groups into the PASP chains, the interaction of the polymer molecules with the mild steel surface increases, and thereby leads to the improved inhibition efficiencies.

3.2.3. Electrochemical impedance spectroscopy measurements. The Nyquist plots of the mild steel in 0.5 M H_2SO_4 solution without and with different inhibitor concentrations are shown in Fig. 5(a and b). The depressed semi-circular shape of the Nyquist plots indicates a non-ideal electrochemical behavior at the solid/liquid interface.[45] In addition, the Nyquist plots obtained without and with inhibitors present a capacitive loop at high frequency and an inductive loop at low frequency. The capacitive loop is related to the double-layer capacitance of the solution and electrode interface. Meanwhile, the inductive loop results from the relaxation of the compounds adsorbed on the electrode surface. The diameter of the Nyquist plot increases with increasing inhibitor concentration, indicating that the impedance of the inhibited substrate increases with increasing inhibitor concentration. Meanwhile, the diameter of the semi-circles obeys the order of PD-1 < PD-2 at the same concentrations, which suggests that the most effective adsorption layer on the mild steel surface was formed in the presence of PD-2 in 0.5 M H_2SO_4 solution, and the aggressive attack by the acidic solution was efficiently blocked.

Bode and phase angle curves for mild steel in 0.5 M H_2SO_4 solution in the absence and presence of inhibitors are displayed in Fig. 6. Only one time constant is observed in the Bode plots, meaning that the corrosion of mild steel in 0.5 M H_2SO_4 solution is mainly controlled by a charge transfer process. At the interface of the metal and solution, the charge distribution on the metal side is controlled by electrons, whereas it is controlled

Table 1 Potentiodynamic polarization parameters extracted from the polarization curves and the corresponding inhibition efficiencies (IE_P) of PD-1 and PD-2 at different concentrations in 0.5 M H_2SO_4 solution at 298 K

Inhibitor	C (mg L^{-1})	$-E_{corr}$ (V *vs.* SCE)	β_a (mV dec^{-1})	$-\beta_c$ (mV dec^{-1})	R_P (Ω cm^2)	i_{corr} (mA cm^{-2})	IE_P (%)	θ
Blank	—	0.475	104.4	136.7	11.5	2.232	—	—
PD-1	5	0.480	62.5	128.2	29.4	0.621	72.2	0.722
	10	0.482	59.7	125.6	38.1	0.461	79.3	0.793
	20	0.481	51.7	126.1	57.3	0.278	87.5	0.875
	50	0.481	49.7	118.6	57.8	0.262	88.3	0.883
	100	0.485	47.3	116.7	61.9	0.237	89.4	0.894
PD-2	5	0.474	53.1	123.9	50.2	0.353	84.1	0.841
	10	0.489	51.0	128.8	63.7	0.249	88.8	0.888
	20	0.489	46.5	123.7	72.9	0.224	90.0	0.900
	50	0.496	52.5	123.2	82.5	0.180	91.9	0.919
	100	0.464	45.4	121.8	119.3	0.134	94.0	0.940

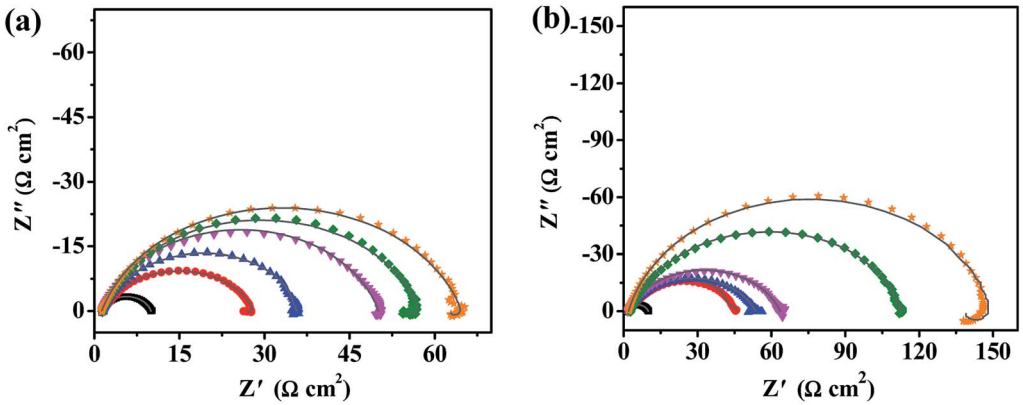

Fig. 5 Nyquist plots and fitted curves (—) for mild steel in 0.5 M H_2SO_4 solution without (■) and with different concentrations of PD-1 (a) and PD-2 (b) at 298 K. Inhibitor concentration: 5 mg L^{-1} (●), 10 mg L^{-1} (▲), 20 mg L^{-1} (▼), 50 mg L^{-1} (◆) and 100 mg L^{-1} (★).

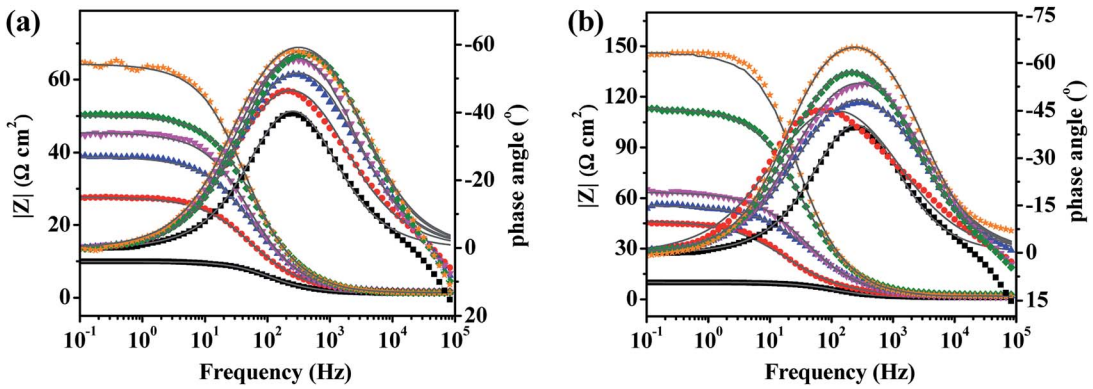

Fig. 6 Bode plots and fitted curves (—) for mild steel in 0.5 M H_2SO_4 solution without (■) and with different concentrations of PD-1 (a) and PD-2 (b) at 298 K. Inhibitor concentration: 5 mg L^{-1} (●), 10 mg L^{-1} (▲), 20 mg L^{-1} (▼), 50 mg L^{-1} (◆) and 100 mg L^{-1} (★).

by the ions on the solution side. Since electrons are much smaller than ions, a differential capacitance is formed rather than an ideal capacitor at the metal/solution interface.[46] Therefore, the impedance curves were modeled using an electrical equivalent circuit which is shown in Fig. 7. The fitted curves for the impedance data are shown in Fig. 5 and 6, respectively. The equivalent circuit model is applied to determine the solution resistance (R_s), constant phase element (CPE), charge transfer resistance (R_{ct}), inductance (L) and the inductance resistor (R_L). The impedance of the CPE can be described *via* the following eqn (3):[40]

$$Z_{CPE} = [Y_0(j\omega)^n]^{-1} \quad (3)$$

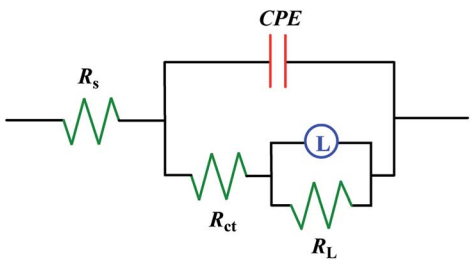

Fig. 7 Equivalent circuit used to fit the EIS data of mild steel.

where Y_0 is a proportionality factor and $j^2 = -1$ is an imaginary number. ω is the angular frequency (in rad s^{-1}), n is the CPE exponent (phase shift), and ω is obtained at the frequency for which the imaginary range of the impedance is a maximum from the following eqn (4):[13]

$$\omega = (Y_0 R_{ct})^{-n} \quad (4)$$

The inhibition efficiencies (IE_E) are calculated using the following eqn (5):

$$IE_E(\%) = \frac{R_{ct} - R_{ct}^0}{R_{ct}} \times 100 \quad (5)$$

where R_{ct} and R_{ct}^0 are the charge transfer resistance in the presence and absence of inhibitor, respectively. The relevant electrochemical impedance data obtained from the equivalent circuit are summarized in Table 2. It is apparent from Table 2 that the value of R_{ct} increases with increasing inhibitor concentration, which indicates that more inhibitor molecules absorb on the mild steel surface and the surface coverage is enhanced.[24] In addition, the phase shift value (n) is almost constant, which indicates that the dissolution mechanism of carbon steel in the solutions with and without corrosion

Table 2 EIS parameters and inhibition efficiencies (IE_E) of PD-1 and PD-2 at different concentrations in 0.5 M H_2SO_4 solution at 298 K

Inhibitor	C (mg L^{-1})	R_s (Ω cm^2)	CPE Y_0 ($\times 10^6$ S^n Ω^{-1} cm^{-2})	n	R_{ct} (Ω cm^2)	R_L (Ω cm^2)	IE_E (%)
Blank	—	1.31	640.9	0.84	8.64	5.0×10^{-7}	—
PD-1	5	1.61	557.5	0.77	25.38	1.25	66.0
	10	1.49	352.3	0.82	34.24	1.48	74.8
	20	1.34	191.1	0.83	48.67	0.17	82.2
	50	1.39	282.1	0.82	53.87	2.23	84.0
	100	1.34	191.5	0.84	63.09	2.18	86.3
PD-2	5	1.95	340.0	0.72	44.75	15.81	80.7
	10	1.83	350.0	0.75	51.74	0.02	84.2
	20	1.69	305.4	0.77	61.96	6.9×10^{-4}	86.1
	50	2.71	164.9	0.81	110.5	2.49	92.2
	100	1.96	112.8	0.86	136.4	11.21	93.7

inhibitors is affected by the charge transfer resistance.[13] Under a certain concentration, inhibition efficiencies of two PASP derivatives calculated by eqn (5) obey the order of PD-2 > PD-1, which is in good agreement with the results of potentiodynamic polarization. The maximum corrosion inhibition efficiency is high as 93.7% in the presence of PD-2 at a low concentration of 100 mg L^{-1}.

3.3. Weight loss measurements

Weight-loss measurement is a classic and highly reliable method to determine the inhibition efficiency of inhibitor. The corrosion rate of mild steel (v_{corr}, g m^{-2} h^{-1}) and inhibition efficiency (IE_W) are calculated by the following eqn (6) and (7),[47] respectively:

$$v_{corr} = \frac{m_0 - m}{Ai \times \Delta t} \quad (6)$$

$$IE_W(\%) = \frac{v^0_{corr} - v_{corr}}{v^0_{corr}} \times 100 \quad (7)$$

where m_0 and m are the weight of mild steel samples before and after immersion in 0.5 M H_2SO_4 solution, Ai is the exposed area, and Δt is the immersion time. v^0_{corr} and v_{corr} are the corrosion rates of mild steel samples without and with the addition of inhibitors. The values of v_{corr} and IE_W for PD-1 and PD-2 at different concentrations are summarized in Table 3. By increasing the concentration of the inhibitors from 5 to 100 mg L^{-1}, the corrosion rate of mild steel decreased and inhibition efficiency was gradually enhanced. It is also seen clearly that the corrosion inhibition efficiencies of PD-2 are higher than those of PD-1 for the entire concentration range from 5 to 100 mg L^{-1}, and this trend is consistent with the results of the electrochemical measurements discussed in the previous section.

Table 3 Corrosion parameters determined from weight-loss tests in 0.5 M H_2SO_4 solution in the absence and presence of various concentrations of inhibitor at 298 K

Inhibitor	C (mg L^{-1})	v_{corr} (g m^{-2} h^{-1})	IE_W (%)
Blank	—	37.99	—
PD-1	5	12.23	67.8
	10	10.75	71.7
	20	9.42	75.2
	50	8.28	78.2
	100	6.04	84.1
PD-2	5	7.10	81.3
	10	6.57	82.7
	20	6.42	83.1
	50	5.01	86.8
	100	3.42	91.0

3.4. Adsorption isotherm

It is well known that organic molecules reduce the corrosion of metal in acidic solutions by adsorbing on the metal surface. The adsorption behavior between the inhibitor molecules and metal surface can be investigated from the adsorption isotherms.[48] In this section, adsorption isotherms, including Frumkin, Temkin and Langmuir isotherms, are applied to fit the surface coverage (θ) values at different concentrations. According to these isotherms, the values of θ as a function of concentrations (C) are represented *via* the following eqn (8)–(10).[49]

$$\left(\frac{\theta}{1-\theta}\right)\exp(2a\theta) = K_{ads}C \text{ (Frumkin isotherm)} \quad (8)$$

$$\exp(-2a\theta) = K_{ads}C \text{ (Temkin isotherm)} \quad (9)$$

$$\frac{C}{\theta} = \frac{1}{K_{ads}} + C \text{ (Langmuir isotherm)} \quad (10)$$

where θ is the surface coverage, which is obtained from inhibition efficiency values and is listed in Table 1; C is the concentration of the inhibitor; K_{ads} is the adsorption equilibrium constant; and "a" is the molecular interaction parameter.

The functional relationships between θ and C are plotted and shown in Fig. 8 (a–c). The correlation coefficient (R^2) is adopted to explore the isotherm that best matches the experimental data. The best fitted straight line is obtained from the plot of C/θ against C, as shown in Fig. 8(c). The value of R^2 is over 0.999 for PD-1 and PD-2, respectively. Therefore, the Langmuir adsorption isotherm is confirmed as the best adsorption model. Then, the adsorption–desorption equilibrium constants (K_{ads}) are obtained from the intercepts of the straight lines, and the results are listed in Table 4. The higher value of K_{ads} suggests the higher coverage rate and thus a better protective layer of the

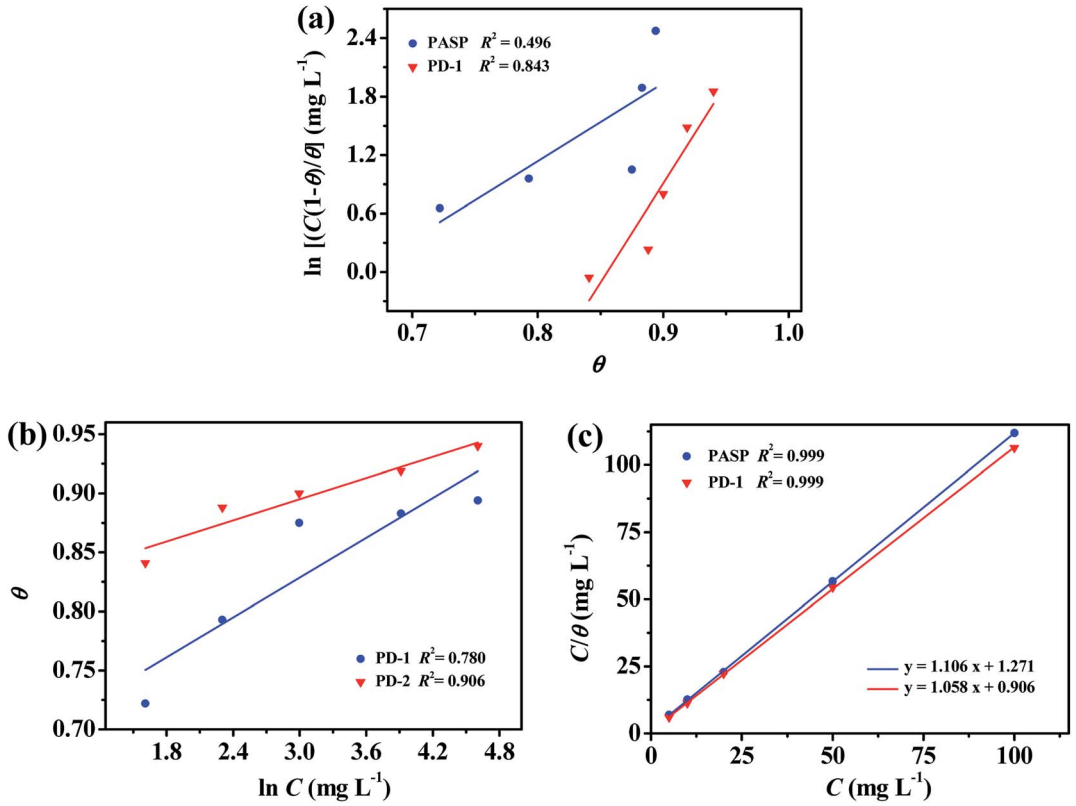

Fig. 8 Frumkin (a), Temkin (b) and Langmuir (c) isotherm plots for mild steel in 0.5 M H_2SO_4 solutions at 298 K containing different concentrations of PD-1 and PD-2.

Table 4 Thermodynamic parameters for the adsorption of PD-1 and PD-2 on mild steel surfaces in 0.5 M H_2SO_4 solution

Inhibitor	R^2	Slope	K_{ads} (L mg^{-1})	$-\Delta G^0$ (KJ mol^{-1})
PD-1	0.999	1.106	0.787	33.635
PD-2	0.999	1.058	1.103	34.472

inhibitors on the mild steel surface.[40,48] As shown in Table 4, the value of K_{ads} of PD-2 is higher than that of PD-1, which is in accordance with the trend of the corrosion inhibition efficiency calculated by electrochemical and weight-loss measurements.

In addition, the value of K_{ads} is related to the standard free energy (ΔG^0_{ads}) of adsorption process by the following eqn (11):[16]

$$\Delta G^0_{ads} = -RT \ln(1 \times 10^6 K_{ads}) \quad (11)$$

where R is the universal gas constant (8.314 J K^{-1} mol^{-1}) and T is the absolute temperature (K). The value of 1×10^6 is the concentration of water molecules expressed in mg L^{-1}. Generally, the value of ΔG^0_{ads} around -20 kJ mol^{-1} is consistent with the electrostatic interaction between the charged metal surface and the charged inhibitor molecules (physisorption), while a negative value of ΔG^0_{ads} less than -40 kJ mol^{-1} usually represents chemisorptions due to the coordinate interactions between lone pair electrons (or π-electrons) in the inhibitor molecule and the charged metal surface.[50] According to Table 4, the values of ΔG^0_{ads} for PD-1 and PD-2 are -33.64 and -34.47 kJ mol^{-1}, respectively. Therefore, the adsorption behaviors of PD-1 and PD-2 are mixed-type involving physisorption and chemisorption. In addition, a more negative ΔG^0_{ads} value with PD-2 as an inhibitor represents a more stable adsorption layer of PD-2 molecules on the steel surface in comparison with that of PD-1.[40]

3.5. Adsorption and inhibition mechanism

Based on the above results and discussion, the adsorption and inhibition mechanisms of PD-1 and PD-2 for mild steel in 0.5 M H_2SO_4 solution were described. First, the mild steel surface becomes electronegative by adsorbing sulfate ions on the surface.[51] With PD-1 as the inhibitor, polyamino acid chains will be protonated in the acidic solution and physically adsorbs on the cathodic sites of the mild steel surface by an electrostatic interaction.[52] Meanwhile, chemisorption of the polymer chains on the mild steel surface may occur *via* donor–acceptor interactions between the p-electrons of N (and/or O) atoms and the vacant d-orbitals of Fe atoms. Besides these interactions relative with PASP chains. PD-1 has additional electrostatic interactions with the negatively charged metal surface due to the protonated imidazole ring, as well as the chemisorption due to the donor–acceptor interaction between the π-electrons and the vacant d-orbitals of Fe. Therefore, PD-1 exhibits better corrosion inhibition efficiency than pure PASP. However, the positive hydrogen ions in the solution can also move to the negatively charged

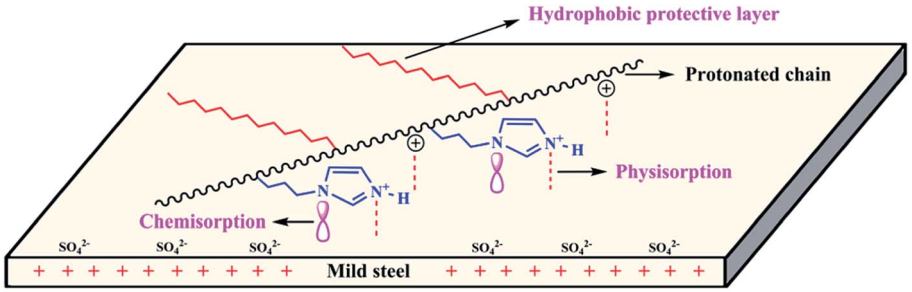

Fig. 9 Schematic illustration of the adsorption behavior of PD-2 on a mild steel surface in 0.5 M H_2SO_4 solution.

metal surface and result in a certain degree of corrosion of the mild steel. Different from PD-1, a hydrophobic long alkyl chain is also bonded onto the molecular chains of PD-2. In addition to the interactions of the polyamino acid chain and imidazole ring with the mild steel surface, long alkyl chains also play an important role in the adsorption and inhibition behaviors.[10] Due to the intrinsic nature of hydrophobic, the long *n*-dodecyl chains in PD-2 will reside on the mild steel surface and cover the metal surface more effectively,[17,53] which can exclude the corrosive ions approaching the mild steel surface. The influence of long alkyl group is the key reason that PD-2 shows superior inhibition efficiency. The schematic illustration of the adsorption behavior of PD-2 on mild steel in 0.5 M H_2SO_4 solution is shown in Fig. 9, from which we can see that there are three types of interactions between PD-2 molecules and the mild steel surface.

3.6. Surface analysis by SEM and EDX

The above discussions clearly show that the inhibition efficiency of the PASP derivative PD-2 for mild steel in 0.5 M H_2SO_4 solution is much better than that of PD-1. To further reveal the corrosion inhibition performance of PD-2, SEM images and EDX spectra of the corroded mild steel surfaces without and with 100 mg L^{-1} of PD-2 immersed in 0.5 M H_2SO_4 solution for 12 h were detected and are shown in Fig. 10(a and b). From Fig. 10(a), the surface is relatively rough and has deep holes, indicating that the mild steel surface is corroded seriously in the blank sulfuric acid solution. The appearance of O and S signals in the EDX spectrum indicates that the corrosion products may be composed of iron oxides and a small amount of iron sulfate.[53,54] In comparison, in the presence of 100 mg L^{-1} PD-2, the mild steel surface shows considerably

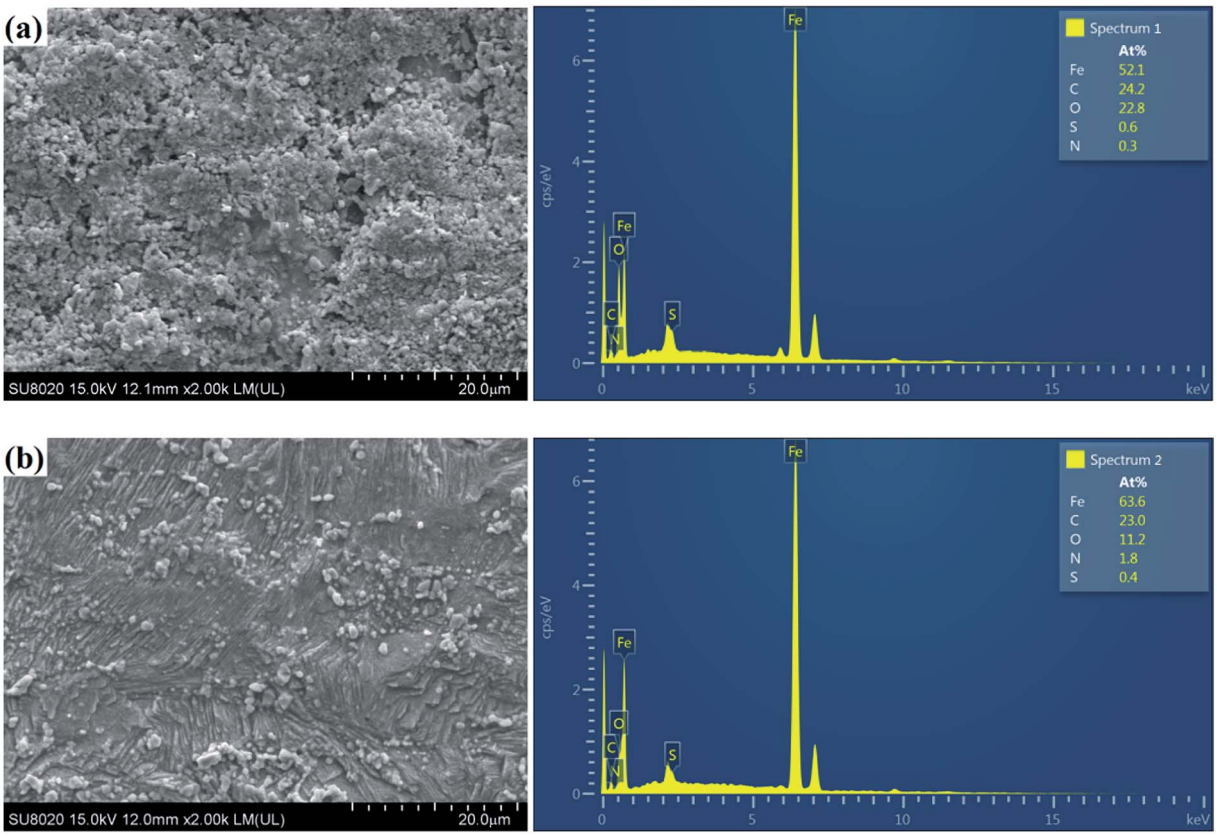

Fig. 10 SEM images and EDX spectra of the mild steel surfaces after 12 h immersion in 0.5 M H_2SO_4 solutions in the absence (a) and presence of 100 mg L^{-1} PD-2 (b).

less corrosion, and some original abrading scratches are also observed (Fig. 10(b)). This could be further confirmed by the decreased content of O and S in the EDX spectrum shown in Fig. 10(b).[55] Meanwhile, it is also seen clearly from EDX spectrum in Fig. 10(b) that the content of N on the mild steel surface is enhanced significantly in the presence of PD-2. Therefore, it is evident that PD-2 molecules adsorb on the mild steel surface and the protective polymer layer effectively retards the corrosion of mild steel in 0.5 M H_2SO_4 solution.

3.7. Surface analysis by XPS

Finally, XPS was carried out to further investigate the composition of the adsorbed film on the steel surface with PD-2 as the inhibitor. Fig. 11 shows the full-range and high-resolution XPS spectra of the mild steel surface after immersion in 0.5 M H_2SO_4 for 12 h in the presence of 100 mg L^{-1} PD-2. The high-resolution C1s spectrum shows three main peaks. The first and most intense peak at 284.8 eV is attributed to the C–H, C–C and C=C bonds in PD-2 and to the presence of contaminant hydrocarbons.[56] The second peak at 286.2 eV is attributed to the C=N

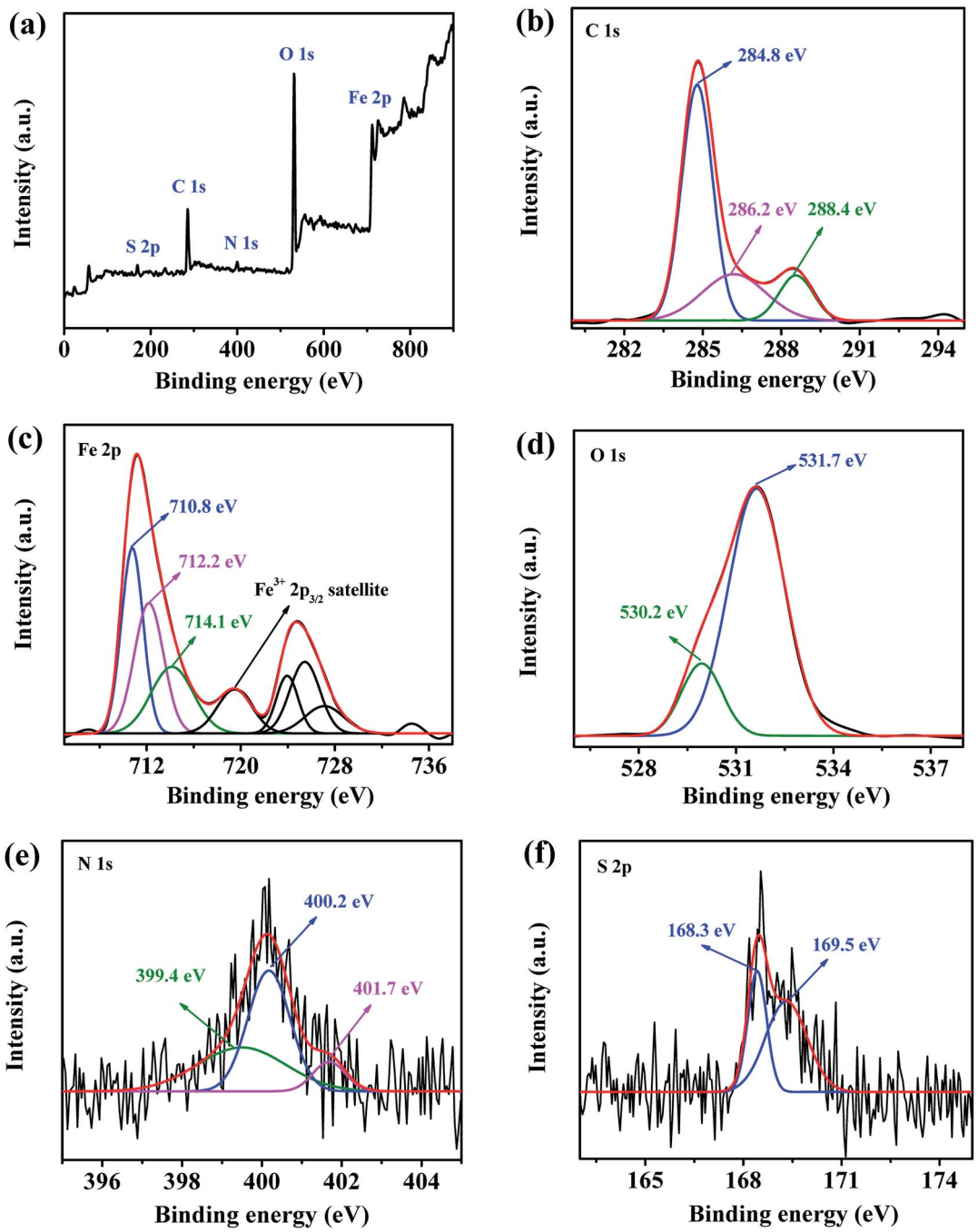

Fig. 11 Full-range spectrum (a) and XPS deconvoluted profiles of C 1s (b), Fe 2p (c), O 1s (d), N 1s (e) and S 2p (f) for mild steel immersed in 0.5 M H_2SO_4 solutions for 12 h at 298 K in the presence of 100 mg L^{-1} PD-2.

and C–N bonds in the amide groups and imidazole rings. The last peak at a higher binding energy (288.4 eV) can be mainly attributed to the N–C=O (imide group) and carbon atom of $–C^{+}–OH$ which is related to the protonation of the carbonyl groups in acid medium.[57]

The spectrum of Fe 2p exhibits two peaks at 711.2 eV (Fe $2p_{3/2}$) and 724.8 eV (Fe $2p_{1/2}$) together with the associated ghost structure. The deconvolution of the Fe $2p_{3/2}$ spectrum consists of four main peaks. The first peak located at 710.8 eV is assigned to Fe_2O_3 and/or Fe–N,[58] while that located at 712.2 eV is attributed to ferric hydroxide such as FeOOH.[59] As discussed by Grosvenor *et al.*,[60] the other two peaks at approximately 714.1 and 719.0 eV are ascribed to the surface peak and the satellite of Fe(III), respectively. The formation of the insoluble layer (Fe_2O_3 and FeOOH) may reduce the ionic diffusion and thus may be beneficial to improving the corrosion resistance of the mild steel surface in 0.5 M H_2SO_4 solution.[58]

The spectrum of O 1s can be fitted into two main peaks as shown in Fig. 11(d). The first peak, observed at 530.2 eV, could be related to the O atoms in the ferric oxides (Fe_2O_3), which is consistent with the presence of the Fe_2O_3/FeOOH layer as detected in the Fe 2p spectrum. The second and most intense peak observed at 531.7 eV is ascribed to the OH^{-} of hydrous iron oxides (FeOOH) and to O–S in the adsorbed sulfate ion (SO_4^{2-}). This peak may also be assigned to O atoms in carbonyl group (C=O).[56]

The deconvolution of N 1s signal could be fitted into three peaks as shown in Fig. 11(e). The first peak located at 399.4 eV is attributed to unprotonated C–N and C=N in the PASP chains and imidazole rings. The second peak located at approximately 400.2 eV is attributed to N atoms coordinated with the mild steel surface (N–Fe).[58] The third peak at 401.7 eV is attributed to $–N^{+}H–$ resulting from the protonation of the N atoms in the amide groups and/or the imidazole rings, which lead to a positive polarization of N atoms and, thereby, an increase in the binding energy.[49] The presence of nitrogen species indicates clearly that PD-2 molecules adsorb on the metal steel surface by chemisorption and physisorption in 0.5 M H_2SO_4 solution.

The S 2p spectrum exhibits two peaks at 168.3 and 169.5 eV for S $2p_{3/2}$ and S $2p_{1/2}$, respectively which can be ascribed to S atoms in SO_4^{2-}.[39] This result reflects the presence of sulfur on the steel surface, and it coincides with the above EDX analysis.

The presence of nitrogen species of the protonated nitrogen atoms ($–N^{+}H–$) and carbon cation structure ($–C^{+}–OH$) on the steel surface confirms that the investigated PASP derivative PD-2 can physically adsorb on the mild steel surface by electrostatic interaction. In addition, the presence of coordinated N and Fe atoms confirms the chemisorption between the PD-2 molecules and the mild steel surface. The results drawn from the XPS analysis provide direct evidence of the adsorption mechanism of PD-2 on the carbon steel surface, as shown in Fig. 9. Because of multiple interactions with the mild steel surface, PD-2 exhibits good inhibition efficiency for mild steel in 0.5 M H_2SO_4 solution.

4. Conclusions

By introducing functional groups into the molecular chains of the eco-friendly polymer PASP, two PASP derivatives (PD-1 and PD-2) were prepared. Their chemical structures were confirmed by FTIR and ^{1}H NMR. Electrochemical measurements and weight loss tests indicate that the inhibition efficiencies of PD-1 and PD-2 are significantly enhanced in comparison with that of PASP. Notably, PD-2 shows an outstanding inhibition performance at low concentrations compared to other polymer inhibitors. At an extremely low concentration of 5 mg L^{-1}, the inhibition efficiency of PD-2 for mild steel in 0.5 M H_2SO_4 solution is up to 84.1%, and a high efficiency of 94.0% can be achieved at a concentration of 100 mg L^{-1} by potentiodynamic polarization measurements. SEM, EDX and XPS analysis clearly show that PD-2 molecules adsorb on the mild steel surface and effectively inhibit corrosion of mild steel in 0.5 M H_2SO_4 solution. Therefore, the new eco-friendly PASP derivative (PD-2) can be expected as a high efficiency polymer inhibitor with low dosage and has potential applications in the fields of acid cleaning, de-scaling and pickling industries.

Conflicts of interest

There are no conflicts to declare.

Acknowledgements

This work was financially supported by Key laboratory for Preparation and Application of Ordered Structural Materials of Guangdong Province (Grant No. KLPAOSM201704).

References

1 M. Goyal, S. Kumar, I. Bahadur, C. Verma and E. E. Ebenso, *J. Mol. Liq.*, 2018, **256**, 565–573.
2 M. A. Deyab, *Desalination*, 2018, **439**, 73–79.
3 M. A. Deyab, K. Eddahaoui, R. Essehli, T. Rhadfi, S. Benmokhtar and G. Mele, *Desalination*, 2016, **383**, 38–45.
4 F. Bentissa, C. Jama, B. Mernari, H. E. Attaria, L. E. Kadi, M. Lebrini, M. Traisnel and M. Lagrenéec, *Corros. Sci.*, 2009, **51**, 1628–1635.
5 I. R. Glasgow, A. J. Rostron and G. Thomson, *Corros. Sci.*, 1966, **6**, 469–482.
6 N. K. Gupta, M. A. Quraishi, C. Verma and A. K. Mukherjee, *RSC Adv.*, 2016, **6**, 102076–102087.
7 A. Dutta, S. K. Saha, P. Banerjee, A. K. Patra and D. Sukul, *RSC Adv.*, 2016, **6**, 74833–74844.
8 Y. Meng, W. Ning, B. Xu, W. Yang, K. Zhang, Y. Chen, L. Li, X. Liu, J. Zheng and Y. Zhang, *RSC Adv.*, 2017, **7**, 43014–43029.
9 X. Li, S. Deng, T. Lin, X. Xie and G. Du, *Corros. Sci.*, 2017, **118**, 202–216.
10 D. Zhang, Y. Tang, S. Qi, D. Dong, H. Cang and G. Lu, *Corros. Sci.*, 2016, **102**, 517–522.
11 M. Ouakki, M. Rbaa, M. Galai, B. Lakhrissi, E. H. Rif and M. Cherkaoui, *Journal of Bio- and Tribo-Corrosion*, 2018, **4**, 35.
12 N. Phadke Swathi, V. D. P. Alva and S. Samshuddin, *Journal of Bio- and Tribo-Corrosion*, 2017, **3**, 46.
13 Z. Salarvand, M. Amirnasr, M. Talebian, K. Raeissi and S. Meghdadi, *Corros. Sci.*, 2017, **114**, 133–145.

14 Z. Hu, Y. Meng, X. Ma, H. Zhu, J. Li, C. Li and D. Cao, *Corros. Sci.*, 2016, **112**, 563–575.
15 A. Singh, K. R. Ansari, J. Haque, P. Dohare, H. Lgaz, R. Salghi and M. A. Quraishi, *J. Taiwan Inst. Chem. Eng.*, 2018, **82**, 233–251.
16 M. T. Alhaffar, S. A. Umoren, I. B. Obot and S. A. Ali, *RSC Adv.*, 2018, **8**, 1764–1777.
17 S.-H. Yoo, Y.-W. Kim, K. Chung, S.-Y. Baik and J.-S. Kim, *Corros. Sci.*, 2012, **59**, 42–54.
18 S. Varvara, R. Bostan, O. Bobis, L. Găină, F. Popa, V. Mena and R. M. Souto, *Appl. Surf. Sci.*, 2017, **426**, 1100–1112.
19 K. Xhanari, M. Finšgar, M. Knez Hrnčič, U. Maver, Ž. Knez and B. Seiti, *RSC Adv.*, 2017, **7**, 27299–27330.
20 N. K. Gupta, P. G. Joshi, V. Srivastava and M. A. Quraishi, *Int. J. Biol. Macromol.*, 2018, **106**, 704–711.
21 F. El-Hajjaji, M. Messali, A. Aljuhani, M. R. Aouad, B. Hammouti, M. E. Belghiti, D. S. Chauhan and M. A. Quraishi, *J. Mol. Liq.*, 2018, **249**, 997–1008.
22 M. Yadav, T. K. Sarkar and I. B. Obot, *RSC Adv.*, 2016, **6**, 110053–110069.
23 S. A. Umoren and U. M. Eduok, *Carbohydr. Polym.*, 2016, **140**, 314–341.
24 B. D. B. Tiu and R. C. Advincula, *React. Funct. Polym.*, 2015, **95**, 25–45.
25 M. Mobin and M. Rizvi, *Carbohydr. Polym.*, 2017, **160**, 172–183.
26 K. Zhang, W. Yang, X. Yin, Y. Chen, Y. Liu, J. Le and B. Xu, *Carbohydr. Polym.*, 2018, **181**, 191–199.
27 R. Karthikaiselvi and S. Subhashini, *J. Mol. Liq.*, 2017, **10**, S627–S635.
28 M. Mobin and M. Rizvi, *Carbohydr. Polym.*, 2017, **156**, 202–214.
29 Y. Sangeetha, S. Meenakshi and C. Sairam Sundaram, *Carbohydr. Polym.*, 2016, **150**, 13–20.
30 B. Zhang, D. Zhou, X. Lv, Y. Xu and Y. Cui, *Desalination*, 2013, **327**, 32–38.
31 A. Zeino, I. Abdulazeez, M. Khaled, M. Jawich and I. Obot, *J. Mol. Liq.*, 2018, **250**, 50–62.
32 L. Yang, Y. Li, B. Qian, B. R. Hou and J. Magnes, *Alloy*, 2015, **3**, 47–51.
33 D. Zeng, T. Chen and S. Zhou, *Int. J. Electrochem. Sci.*, 2015, **10**, 9513–9527.
34 R. Cui, N. Gu and C. Li, *Mater. Corros.*, 2011, **62**, 362–369.
35 B. Qian, J. Wang, M. Zheng and B. Hou, *Corros. Sci.*, 2013, **75**, 184–192.
36 S. M. Tawfik, *J. Mol. Liq.*, 2015, **207**, 185–194.
37 B. N. Tran, Q. T. Bui, Y. S. Jeon, H. S. Park and J.-H. Kim, *Polym. Bull.*, 2015, **72**, 2605–2620.
38 J.-l. Huang, Y.-l. Zhang, Z.-h. Cheng and H.-c. Tao, *J. Appl. Polym. Sci.*, 2007, **103**, 358–364.
39 P. Mourya, P. Singh, A. K. Tewari, R. B. Rastogi and M. M. Singh, *Corros. Sci.*, 2015, **95**, 71–87.
40 L. L. Liao, S. Mo, H. Q. Luo, Y. J. Feng, H. Y. Yin and N. B. Li, *Corros. Sci.*, 2017, **124**, 167–177.
41 S. Banerjee, V. Srivastava and M. M. Singh, *Corros. Sci.*, 2012, **59**, 35–41.
42 H. M. Abd El-Lateef, M. A. Abo-Riya and A. H. Tantawy, *Corros. Sci.*, 2016, **108**, 94–110.
43 M. Srimathi, R. Rajalakshmi and S. Subhashini, *J. Mol. Liq.*, 2014, **7**, 647–656.
44 S. A. Umoren, I. B. Obot, A. Madhankumar and Z. M. Gasem, *Carbohydr. Polym.*, 2015, **124**, 280–291.
45 X. Luo, X. Pan, S. Yuan, S. Du, C. Zhang and Y. Liu, *Corros. Sci.*, 2017, **125**, 139–151.
46 N. Yilmaz, A. Fitoz, ÿ. Ergun and K. C. Emregül, *Corros. Sci.*, 2016, **111**, 110–120.
47 Y. Zhou, L. Guo, S. Zhang, S. Kaya, X. Luo and B. Xiang, *RSC Adv.*, 2017, **7**, 23961–23969.
48 M. A. Bedair, M. M. B. El-Sabbah, A. S. Fouda and H. M. Elaryian, *Corros. Sci.*, 2017, **128**, 54–72.
49 M. Bouanis, M. Tourabi, A. Nyassi, A. Zarrouk, C. Jama and F. Bentiss, *Appl. Surf. Sci.*, 2016, **389**, 952–966.
50 M. Mobin, S. Zehra and R. Aslam, *RSC Adv.*, 2016, **6**, 5890–5902.
51 K. R. Ansari, M. A. Quraishi and A. Singh, *Corros. Sci.*, 2015, **95**, 62–70.
52 H. T. M. Abdel-Fatah, M. M. Kamel, A. A. M. Hassan, S. A. M. Rashwan, S. M. Abd El Wahaab and H. E. E. El-Sehiety, *J. Mol. Liq.*, 2017, **10**, S1164–S1171.
53 S. A. Ali, A. M. El-Shareef, R. F. Al-Ghamdi and M. T. Saeed, *Corros. Sci.*, 2005, **47**, 2659–2678.
54 N. V. Likhanova, M. A. Domínguez-Aguilar, O. Olivares-Xometl, N. Nava-Entzana, E. Arce and H. Dorantes, *Corros. Sci.*, 2010, **52**, 2088–2097.
55 A. Pourghasemi Hanza, R. Naderi, E. Kowsari and M. Sayebani, *Corros. Sci.*, 2016, **107**, 96–106.
56 A. Zarrouk, B. Hammouti, T. Lakhlifi, M. Traisnel, H. Vezin and F. Bentiss, *Corros. Sci.*, 2015, **90**, 572–584.
57 J. Morgan, A. Greenberg and J. F. Liebman, *Struct. Chem.*, 2011, **23**, 197–199.
58 B. Zhang, C. He, C. Wang, P. Sun, F. Li and Y. Lin, *Corros. Sci.*, 2015, **94**, 6–20.
59 H. Tian, W. Li, B. Hou and D. Wang, *Corros. Sci.*, 2017, **117**, 43–58.
60 A. P. Grosvenor, B. A. Kobe, M. C. Biesinger and N. S. McIntyre, *Surf. Interface Anal.*, 2004, **36**, 1564–1574.